Solar Physics
DOI: 10.1007/•••••-•••-•••-••••-•

On the Relationship between Equilibrium Bifurcations and Ideal MHD Instabilities for Line-Tied Coronal Loops

T. Neukirch[1] · **Z. Romeou**[1,2]

Abstract

For axisymmetric models for coronal loops the relationship between the bifurcation points of magnetohydrodynamic (MHD) equilibrium sequences and the points of linear ideal MHD instability is investigated imposing line-tied boundary conditions. Using a well-studied example based on the Gold-Hoyle equilibrium, it is demonstrated that if the equilibrium sequence is calculated using the Grad-Shafranov equation, the instability corresponds to the second bifurcation point and not the first bifurcation point because the equilibrium boundary conditions allow for modes which are excluded from the linear ideal stability analysis. This is shown by calculating the bifurcating equilibrium branches and comparing the spatial structure of the solutions close to the bifurcation point with the spatial structure of the unstable mode. If the equilibrium sequence is calculated using Euler potentials the first bifurcation point of the Grad-Shafranov case is not found, and the first bifurcation point of the Euler potential description coincides with the ideal instability threshold. An explanation of this results in terms of linear bifurcation theory is given and the implications for the use of MHD equilibrium bifurcations to explain eruptive phenomena is briefly discussed.

Keywords: Magnetohydrodynamics; Instabilities; Corona, Structures; Flares, Relation to Magnetic Field

1. Introduction

Magnetohydrodynamic instabilities of coronal loops are since a long time discussed as one of the main theoretical explanations for solar flares, in particular compact loop flares (*e.g.* Priest, 1982). Traditionally, investigations of MHD instabilities of coronal loops model these loops as straight cylindrical flux tubes

[1] School of Mathematics and Statistics, University of St. Andrews, St. Andrews, KY16 9SS, United Kingdom email: thomas@mcs.st-and.ac.uk
[2] Now at: Ministry of Development, Department of Metrology, Cannigos Square, 101 81 Athens, Greece, email: zrom@gge.gr

of finite length with line tied boundary conditions at the 'photospheric' ends of the flux tubes (*e.g.* Raadu, 1972; Hood and Priest, 1979, 1981; Einaudi and Van Hoven, 1983; Velli *et al.*, 1990). Such a set-up allows for a wide variety of relatively simple equilibrium configurations, hence explaining its popularity.

The stability of equilibrium configurations of the above mentioned type has been studied for several decades using the methods of linear MHD stability analysis (*e.g.* Raadu, 1972; Hood and Priest, 1979, 1981; Einaudi and Van Hoven, 1983; Velli *et al.*, 1990; De Bruyne and Hood, 1989, 1992; Mikić *et al.*, 1990; Hood *et al.*, 1994; van der Linden and Hood, 1998, 1999). In recent years the investigations have been extended into the nonlinear regime using large-scale MHD simulations (*e.g.* Longbottom *et al.*, 1996; Baty and Heyvaerts, 1996; Baty, 1997a, 1997b, 2000a, 2000b; Lionello *et al.*, 1998; Arber *et al.*, 1999; Gerrard *et al.*, 2001; Browning and Van der Linden, 2003; Browning *et al.*, 2008; Hood *et al.*, 2009).

In the present contribution we want to investigate the stability of line-tied coronal loop models from a different point of view. The flux tube equilibria used to model coronal loops all depend on one or more parameters representing quantities like the magnetic twist or the plasma beta. Many investigations study how the linear stability of the loops changes as one (or more) of these equilibrium parameters vary.

The systematic variation of one or several parameters of an equilibrium defines an equilibrium sequence, and a point of linear instability should correspond to a bifurcation point of the equilibrium sequence and vice versa. It has to be kept in mind, however, that magnetostatic equilibria are usually calculated by solving a mathematically reduced set of equations. It is not at all clear whether there is really a one-to-one correspondence between points of linear instability and bifurcation points, in particular if line-tied boundary conditions are imposed as in models of coronal loops.

In the present paper we shall investigate the question whether the points of linear instability of rotationally symmetric straight line-tied flux tubes have a one-to-one correspondence with the bifurcation points of equilibrium sequences.

We shall use two different ways of calculating the equilibrium sequences, namely Grad-Shafranov theory and Euler potentials, and we shall, for simplicity, investigate only axisymmetric instabilities and bifurcations. A particularly well-studied equilibrium class (Gold and Hoyle, 1960) will be used to carry out this investigation, mainly because results of linear stability investigations for this equilibrium class are readiliy available in the literature (*e.g.* Hood and Priest, 1979, 1981; Mikić *et al.*, 1990; De Bruyne and Hood, 1992).

In Section 2 the basic equilibrium theory and those parts of the theory of linear MHD stability needed in this paper are discussed. The following Section 3 presents a brief outline of the numerical method used to calculate the equilibrium sequences and to determine their bifurcation points and bifurcating branches. The results of these calculations are given in Section 4 and discussed in Section 5. The paper closes with a summary in Section 6.

2. Basic Theory

2.1. The Gold-Hoyle Equilibrium

We start our investigation from static equilibrium solutions of the MHD equations, *i.e.* solutions of

$$\mathbf{j} \times \mathbf{B} - \nabla p = \mathbf{0} \tag{1}$$
$$\nabla \times \mathbf{B} = \mu_0 \mathbf{j} \tag{2}$$
$$\nabla \cdot \mathbf{B} = 0. \tag{3}$$

We are looking for solutions in cylindrical coordinates r, ϕ, z, and restrict the spatial domain to $0 \leq z \leq L$. The solutions will be considered as straight flux tube approximations of coronal loops, in the sense of a large aspect ratio expansion. In this case L is the loop length and the boundaries $z = 0$ and $z = L$ have to be identified with the photospheric end points of the loop. The centre of the loop is given by $r = 0$. In the present paper we will only consider solutions which do not depend on ϕ, *i.e.* axisymmetric solutions.

We normalise the magnetic field to the value of B_z in the centre of the loop ($r = 0$), B_0, the coordinates and the loop length by a typical radial length scale, b, and the pressure by B_0^2/μ_0. In this normalisation, the Gold-Hoyle equilibrium (Gold and Hoyle, 1960) is given by the magnetic field components (see *e.g.* Longbottom *et al.*, 1996)

$$B_r = 0, \tag{4}$$
$$B_\phi = \frac{r}{1+r^2}, \tag{5}$$
$$B_z = \frac{\lambda}{1+r^2}, \tag{6}$$

and the plasma pressure

$$p = \frac{1}{2}\frac{1-\lambda^2}{(1+r^2)^2}. \tag{7}$$

The parameter λ controls both the field line twist Φ between $z = 0$ and $z = L$,

$$\Phi = \frac{L}{\lambda} \tag{8}$$

and the plasma beta. For $\lambda = 1$, the equilibrium is force-free, *i.e.* the current density is parallel to the magnetic field lines, whereas for $\lambda = 0$ the current density is everywhere perpendicular to the magnetic field lines. For values of λ between 0 and 1 we have a combination of field-aligned and perpendicular current density. The equilibrium class is not defined for $\lambda > 1$ because the pressure would become negative in this case.

The Gold-Hoyle equilibrium class depends only on the variable r and is therefore a one-dimensional MHD equilibrium. One-dimensional equilibria of this type can be easily calculated (see *e.g.* Priest, 1982, chapter 3.3) We use it

here as a kind of prototype flux tube equilibrium, because linear stability results are readily available for the Gold-Hoyle equilibrium class (De Bruyne and Hood, 1992). To obtain genuinely two-dimensional equilibria depending on r and z we have to resort to one of the more general theories described in the next sections.

2.2. Grad-Shafranov Theory

To satisfy the solenoidal condition (3), we write the magnetic field in the form

$$\mathbf{B} = \frac{1}{r}\nabla A \times \mathbf{e}_\phi + B_\phi \mathbf{e}_\phi. \tag{9}$$

Here the flux function A and the ϕ-component of the magnetic field depend only on r and z. Taking the scalar product of Equation (1) with $\mathbf{B}$ and using the fact that under the condition of axisymmetry the pressure also depends only on r and z, we find that the pressure is a function of A :

$$p(r,z) = F(A(r,z)). \tag{10}$$

An investigation of the ϕ-component of (1) shows that

$$b_\phi(r,z) = rB_\phi(r,z,) = G(A(r,z)) \tag{11}$$

is also a function of A only.

The force balance equation can then be reduced to a single partial differential equation for A (*e.g.* Bateman, 1978) :

$$-r\nabla\cdot\left(\frac{1}{r^2}\nabla A\right) = r\frac{dp}{dA} + \frac{1}{r}b_\phi\frac{db_\phi}{dA}. \tag{12}$$

The dependence of the pressure and the ϕ-component of the magnetic field on the flux function A have to be specified for a solution of this equation. For the Gold-Hoyle solution the flux function A is given by

$$A_{\rm GH}(r,z) = \frac{\lambda}{2}\ln(1+r^2). \tag{13}$$

Using equation (13) to determine r as a function of A, and substituting this expression into Equations (5) and (6) we find that

$$p = \frac{1}{2}(1-\lambda^2)\exp\left(-\frac{4}{\lambda}A\right), \tag{14}$$

$$b_\phi = 1-\exp\left(-\frac{2}{\lambda}A\right). \tag{15}$$

For each value of λ, the Gold-Hoyle equilibrium is therefore a solution of the Grad-Shafranov equation

$$\begin{aligned} -\frac{\partial}{\partial r}\left(\frac{1}{r}\frac{\partial A}{\partial r}\right) - \frac{1}{r}\frac{\partial^2 A}{\partial z^2} &= -2r\frac{1-\lambda^2}{\lambda}\exp\left(-\frac{4}{\lambda}A\right) \\ &\quad + \frac{2}{\lambda r}\left[1-\exp\left(-\frac{2}{\lambda}A\right)\right]\exp\left(-\frac{2}{\lambda}A\right), \end{aligned} \tag{16}$$

if the boundary conditions at $z = 0$ and $z = L$ are given by $A = \lambda/2 \ln(1 + r^2)$ as well. As the Gold-Hoyle solutions depend on the parameter λ they define a solution branch of the Grad-Shafranov Equation (16). As this equation is nonlinear it is to be expected that it can also have other solution branches for the same boundary conditions. Points where the Gold-Hoyle solution branch and any other solution branches meet are called bifurcation points. Standard bifurcation theory (*e.g.* Iooss and Joseph, 1980) tells us that at bifurcation points the stability of the solution branches can change. We will discuss this possibility in more detail in Section 2.4.

2.3. Euler Potentials

The Grad-Shafranov theory is very useful for symmetric plasma systems, but a Grad-Shafranov type equation can only be derived for translational, rotational and helical symmetry (Solovev, 1967; Edenstrasser, 1980a, 1980b). Without such a symmetry, we have to use a different way to calculate MHD equilibria. The approach coming closest to the use of a flux function for symmetric systems is to use Euler potentials (sometimes also called Clebsch coordinates) to describe the magnetic field. The Euler potential approach has the advantage that it can be used to describe three dimensional magnetic fields without symmetry, although there are some restrictions concerning the existence of Euler potentials for given magnetic fields (*e.g.* Hesse, 1988; Rosner *et al.*, 1989). For the flux tube like equilibria considered in the present paper these constraints do not apply.

Another reason for using Euler potentials even for symmetric cases is that certain types of constraints are a lot easier to impose with Euler potentials then with a Grad-Shafranov description. A typical example from solar physics is the quasi-static shearing of magnetic arcades. In this case the footpoint displacement of the fieldlines is the physical parameter which is determined by the boundary conditions. In this case the use of Euler potentials is very useful (*e.g.* Barnes and Sturrock, 1972; Zwingmann, 1987; Platt and Neukirch, 1994; Antiochos *et al.*, 1999).

With the Euler potentials α and β a general magnetic field can be written as

$$\mathbf{B} = \nabla\alpha \times \nabla\beta. \tag{17}$$

Any vector field of this form is automatically solenoidal. In the present paper we restrict our analysis to axisymmetric fields. In this case the Euler potential α is a function of r and z only, the Euler potential β is chosen as $\beta(r, \phi, z) = \tilde{\beta}(r, z) + \phi$ and Equation (17) reduces to

$$\mathbf{B} = \frac{1}{r}\nabla\alpha \times \mathbf{e}_\phi + \nabla\alpha \times \nabla\tilde{\beta}. \tag{18}$$

By comparison with Equation (9), we see that now the Euler potential α corresponds to the flux function A, whereas B_ϕ has been replaced by the $\nabla\alpha \times \nabla\tilde{\beta}$. Substitution of Equation (18) into Equation (1) and (2) gives the two equations

for α and $\tilde{\beta}$ (*e.g.* Zwingmann, 1987; Platt and Neukirch, 1994) :

$$\nabla\tilde{\beta}\cdot\nabla\times(\nabla\alpha\times\nabla\tilde{\beta})-\nabla\cdot\left(\frac{1}{r^2}\nabla\alpha\right) = \frac{dp}{d\alpha}, \tag{19}$$

$$\nabla\alpha\cdot\nabla\times(\nabla\tilde{\beta}\times\nabla\alpha) = 0. \tag{20}$$

For the Gold-Hoyle solution $\alpha_{\rm GH}$ is identical with the flux function $A_{\rm GH}$ given in Equation (13). The pressure function $p(\alpha)$ has the same form as $p(A)$ in Equation (14), only with α replacing A. We can use B_ϕ to work out that for the Gold-Hoyle solution

$$\tilde{\beta}_{\rm GH}=-\frac{1}{\lambda}z. \tag{21}$$

The function $\tilde{\beta}$ represents the fieldline twist for the Gold-Hoyle solution since

$$\tilde{\beta}_{\rm GH}(r,0)-\tilde{\beta}_{\rm GH}(r,L)=\frac{L}{\lambda}=\Phi \tag{22}$$

We impose boundary conditions for both Euler potentials. The boundary conditions for α are the same as for A in the Grad-Shafranov case. For $\tilde{\beta}$ we use Equation (21) on the boundaries. This fixes the footpoint displacement of fieldlines crossing the boundaries $z=0$ and $z=L$. In the same way as in the Grad-Shafranov case the Gold-Hoyle solutions are a solution branch for the Equations (19) and (20). The same statements about bifurcations and stability apply as in the Grad-Shafranov case.

2.4. Linear Stability

The theory of linear MHD stability is a vast area and we only summarise some results which are important for the following discussion. Defining the Lagrangian displacement $\boldsymbol{\xi}$ the linearized ideal MHD equations can be written as

$$\rho_0\frac{\partial^2\boldsymbol{\xi}}{\partial t^2}=\mathbf{F}(\boldsymbol{\xi}) \tag{23}$$

where

$$\mathbf{F}(\boldsymbol{\xi})=\frac{1}{\mu_0}[(\nabla\times\mathbf{B}_1)\times\mathbf{B}_0]+\frac{1}{\mu_0}[(\nabla\times\mathbf{B}_0)\times\mathbf{B}_1]+\nabla(\boldsymbol{\xi}\cdot\nabla p_0+\gamma p_0\nabla\cdot\boldsymbol{\xi}). \tag{24}$$

The components of the magnetic field perturbation $\mathbf{B}_1$ are given by

$$\mathbf{B}_1=\nabla\times(\boldsymbol{\xi}\times\mathbf{B}_0). \tag{25}$$

For the problem we are discussing in the present paper Equation (23) has to be solved on a tube-like domain with line-tying boundary conditions at $z=0$ and $z=L$, with $\mathbf{B}_0$ and p_0 given by the Gold-Hoyle solution. The line-tying condition corresponds to

$$\boldsymbol{\xi}=\mathbf{0} \tag{26}$$

on the boundaries. Assuming an exponential time-dependence for the perturbation $\boldsymbol{\xi}$, one obtains a self-adjoined eigenvalue problem. Instabilities occur when one of the eigenvalues of the equation changes sign. The corresponding perturbations $\boldsymbol{\xi}$ can be classified according to their different spatial structure. In general we speak of different modes when refering to the spatial structure of the instabilities. For each mode it is usually sufficient to investigate the largest eigenvalue corresponding to this mode, as it is this eigenvalue which determines whether a mode is stable or unstable.

It can be shown that the Gold-Hoyle solution is always stable for $\lambda = 1$, *i.e.* in the force-free case. When decreasing λ the value of λ where the Gold-Hoyle solutions become unstable to the different possible modes under line-tying boundary conditions depends on the length of the flux tube L. A thorough investigation of this problem has been carried out by De Bruyne and Hood (1992) and we will make use of their results in the later parts of this paper. Since we investigate only axisymmetric equilibria and bifurcations we will also restrict our attention to the axisymmetric modes (sometimes called "sausage modes").

3. Numerical Method

The numerical calculations have been carried out with a code based on a continuation method (*e.g.* Allgower and Georg, 1990). The code used here is based on a method proposed by Keller (1977) and has been successfully applied to a variety of problems in plasma physics, solar physics, magnetospheric physics and astrophysics (*e.g.* Zwingmann, 1983, 1987; Neukirch, 1993a, 1993b; Neukirch and Hesse, 1993; Platt and Neukirch, 1994; Schröer *et al.*, 1994; Becker *et al.*, 1996, 2001; Romeou and Neukirch, 1999, 2001, 2002a, 2002b; Kiessling and Neukirch, 2003). The method has the advantage that it can calculate sequences of equilibria depending on an external parameter (like λ for the Gold-Hoyle solutions), and detect bifurcation points. It is also possible to calculate bifurcating equilibrium sequences. The code uses a finite element discretization allowing for a flexible grid structure. Further details can be found in Neukirch (1993a) and Neukirch (1993b) .

We have solved both the Grad-Shafranov Equation (16) and the Euler potential Equations (19) and (20) on a numerical domain extending from $r = 0$ to $r = 8$ and from $z = 0$ to $z = L$, where L is varied between 3 and 8. The radial extent of the domain is chosen along the same lines as done by Longbottom *et al.* (1996) in their MHD simulations of the sausage instability.

For the Grad-Shafranov equilibrium sequences we have used

$$A_b = A_{\rm GH} \tag{27}$$

as boundary condition on all boundaries. In the Euler potential case the boundary conditions are given by

$$\alpha_b = A_{\rm GH}, \tag{28}$$

$$\tilde{\beta}_b = \tilde{\beta}_{\rm GH}. \tag{29}$$

Note that in both cases both the differential equation and the boundary conditions depend on the parameter λ. Due to the boundary conditions the Gold-Hoyle solutions are one solution branch of the equations. This can be used to check the accuracy of the numerical code and to adjust the resolution. In all runs presented in Section 4 we have used a numerical grid with 1800 triangular finite elements corresponding to a resolution of 61 by 61 grid points in each spatial direction. The grid is equidistant in the z-direction but non-equidistant in the r-direction with a higher resolution towards the axis of the tube.

4. Results

For both the Grad-Shafranov and the Euler potential case we have carried out a numerical investigation of the bifurcation properties of the Gold-Hoyle solution branch using the numerical method described in Section 3. For a series of values of the loop length L, we have first calculated the Gold-Hoyle branch with our code, starting with the force-free solution ($\lambda = 1$) and then following the branch for decreasing λ into the non-force-free regime. Although we know the Gold-Hoyle branch analytically this procedure allows us to check the accuracy of our numerical calculations and to use the capability of the code to detect bifurcation points. At such points other solution branches cross the Gold-Hoyle branch, and we expect that those points correspond to the instability threshold of the $m = 0$-instability under line-tying conditions as, for example, calculated by De Bruyne and Hood (1992) . For the detected bifurcation points we have then also calculated the bifurcating branches for a range of λ values. This is important to check whether the spatial structure of the bifurcating solution branch coincides with the predictions made by linear stability theory on the basis of the structure of the unstable mode.

An important point to emphasize here is that because we calculate the Gold-Hoyle branch in the direction of decreasing λ, we will also number the bifurcation points in this direction, *i.e.* when we speak of first and second bifurcation the λ value of the first bifurcation will be bigger than the λ value of the second bifurcation. Although this is opposite to the terminology normally used in bifurcation theory, we have decided to keep the parametrization used by De Bruyne and Hood (1992) to make a comparison with their results easier.

4.1. The Grad-Shafranov Case

We have carried out calculations of the Gold-Hoyle branch for loop lenghts $L =$ 3.0, 4.0, 5.0, 6.0, 7.0, 8.0, 9.0 and 10.0. In all cases, we have calculated the Gold-Hoyle branch until we had found at least two bifurcation points. The λ values of the two first bifurcation points found by code for the different L values are listed in Table 1. A graphical representation of these values is shown in Figure 1. In this figure we plot the values for the first and second bifurcation points in the L-λ-plane. Also shown in Figure 1 is the stability threshold for the $m = 0$-instability (dashed line) derived by De Bruyne and Hood (1992) using linear MHD theory. The figure clearly shows that the linear stability threshold

Table 1. The first and second bifurcation points for the Grad-Shafranov case.

L	3.0	4.0	5.0	6.0	7.0	8.0	9.0	10.0
λ_1	0.598	0.629	0.652	0.663	0.675	0.684	0.684	0.690
λ_2	0.472	0.528	0.566	0.593	0.612	0.627	0.639	0.648

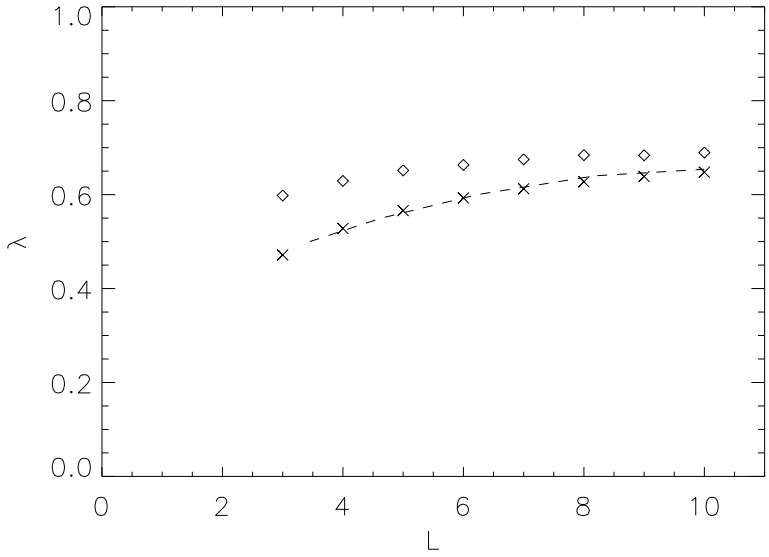

Figure 1. The dependence of the λ values of the first ($\Diamond$) and the second ($\times$) bifurcation point on the loop length L for the Grad-Shafranov case. The dashed line is the instability threshold of the $m = 0$ mode derived by De Bruyne and Hood (1992) using linear MHD stability theory under line-tying conditions. Solutions with λ values below the dashed line are unstable with respect to the sausage mode. It is obvious that the second and not the first bifurcation point for a given loop length corresponds to the $m = 0$ instability.

corresponds to the second bifurcation along the Gold-Hoyle branch. This raises the question what the first bifurcation point corresponds to.

To answer this question, we have calculated the bifurcating branches for the first and second bifurcation points for loop lengths of $L = 3.0$, 5.0 and 7.0. The structure of the bifurcation diagrams is very similar for all three cases and we therefore only show the case $L = 7.0$ (Figure 2). The four quantities shown in Figure 2 are the polodial magnetic energy

$$W_{\rm p} = \int \frac{1}{2} \left(\frac{1}{r} \nabla A \right)^2 dV, \tag{30}$$

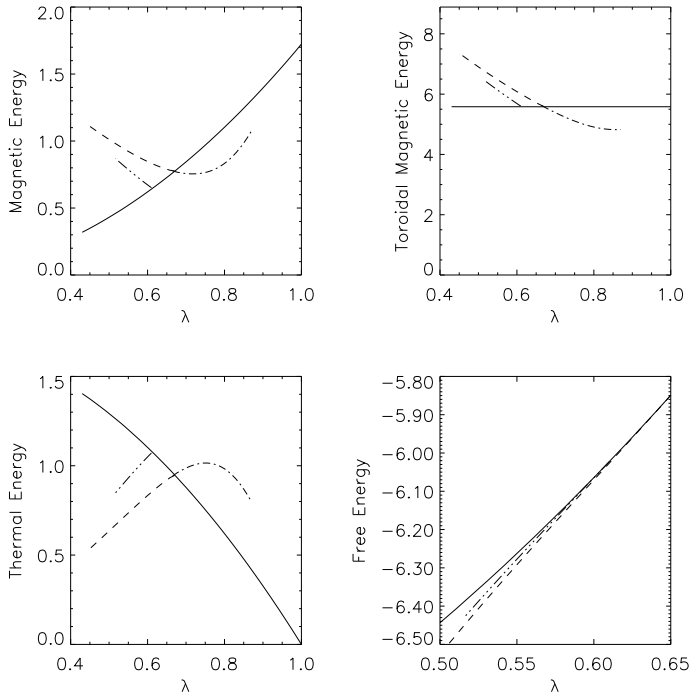

Figure 2. Bifurcation diagrams of the Grad-Shafranov case for $L = 7.0$. Shown are the poloidal magnetic energy (upper left), the toroidal magnetic energy (upper right), the thermal energy (lower left), and the free energy as defined by Grad (1964) (lower right). For definitions of these quantities see the main text. The free energy is only shown for values of λ close to the second bifurcation point to make the difference between the branches more obvious.

the toroidal magnetic energy

$$W_{\rm t} = \int \frac{1}{2} \left(\frac{1}{r} b_\phi \right)^2 dV, \tag{31}$$

the thermal energy

$$W_{\rm th} = \int p \, dV, \tag{32}$$

and the free energy defined by Grad (1964)

$$W_{\rm f} = W_{\rm p} - (W_{\rm t} + W_{\rm th}). \tag{33}$$

At the first bifurcation point another solution branch crosses the Gold-Hoyle branch. The bifurcating branch exists for values of λ both smaller and larger than the bifurcation point λ. At the bifurcation point the poloidal and toroidal magnetic energies of the bifurcating branch go from values smaller than the energies of the Gold-Hoyle branch to values larger than the Gold-Hoyle branch

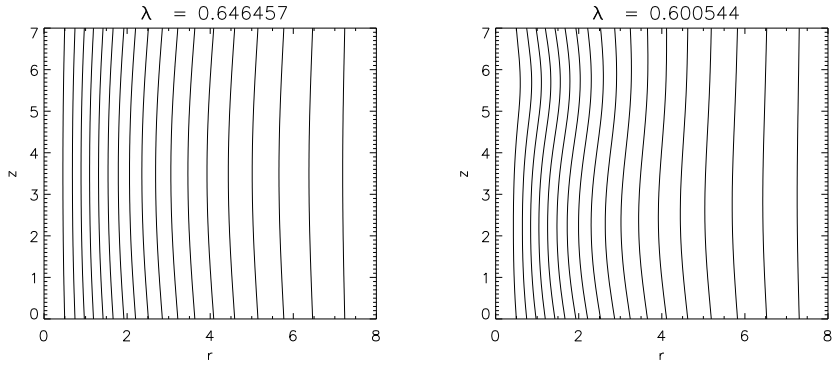

Figure 3. Left: Solution for $\lambda = 0.646457$ on first bifurcating branch. Right: Solution for $\lambda = 0.600544$ on second bifurcating branch. Whereas the solutions on the first bifurcating branch show a $\sin(\pi z/L)$-dependence superimposed on the Gold-Hoyle solution, the solutions on the second bifurcating branch have a $\sin(2\pi z/L)$-dependence.

in the direction of decreasing λ. The thermal energy of the bifurcating branch is higher than that of the Gold-Hoyle branch for λ larger than the bifurcation λ and smaller than the Gold-Hoyle branch beyond the bifurcation point.

The second bifurcating solution branch only exists for values of λ which are smaller than the bifurcation λ. This is to be expected on the basis of standard bifurcation theory (*e.g.* Iooss and Joseph, 1980), taking the spatial structure of the solutions along the branch into account (see below). The mathematical argumentation is given in the Appendix. The poloidal and toroidal magnetic energies along this branch are larger than those of the Gold-Hoyle branch, whereas the thermal energy is smaller than the thermal energy of the Gold-Hoyle branch for the same value of λ.

Also shown in Figure 2 is a plot of the free energy for values of λ close to the second bifurcation point to enhance the difference between the branches. We can see that in this range the Gold-Hoyle branch has the biggest free energy. The first bifurcating branch has lower free energy than the second branch but both branches have a lower free energy than the Gold-Hoyle branch. This shows that a transition to the bifurcating branches at fixed λ is indeed energetically favourable for the system, as the system will always try to settle into a state of lower free energy.

The spatial structure of the solutions on the bifurcating branches is shown in Figure 3. The obvious difference between the solutions on the two branches is their dependence on z. Whereas the solutions on the first bifurcating branch show a $\sin(\pi z/L)$-dependence superimposed on the Gold-Hoyle solution, the solutions on the second bifurcating branch have a $\sin(2\pi z/L)$-dependence. Both functions are consistent with the boundary condition $A = A_{\rm GH}$ at $z = 0$ and $z = L$. We will discuss the implications of this finding in the light of linear stability theory in Section 5.

Table 2. The first bifurcation point for the Euler potential case.

L	3.0	4.0	5.0	6.0	7.0	8.0	9.0	10.0
λ_1	0.472	0.528	0.566	0.593	0.613	0.628	0.639	0.648

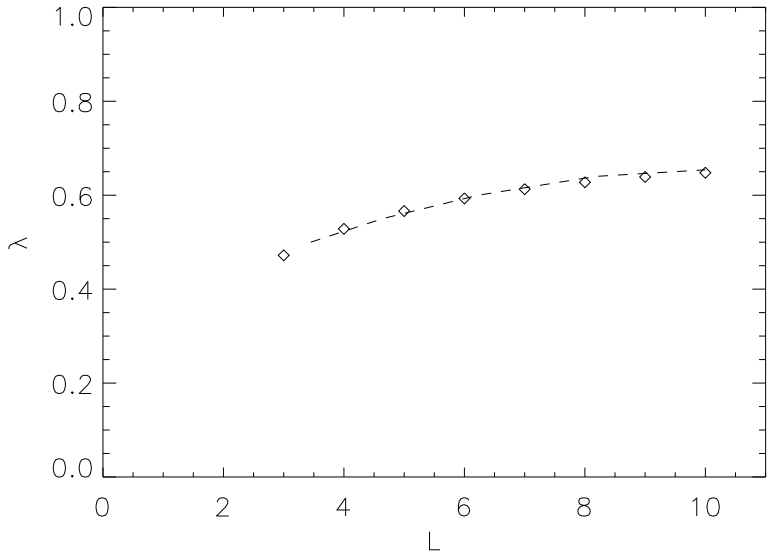

Figure 4. The dependence of the λ values on the loop length L for the Euler potential case. The Euler potential case is different from the Grad-Shafranov case because in this case the first ($\Diamond$) bifurcation point corresponds to the point where the $m = 0$-mode becomes unstable.

4.2. The Euler Potential Case

In the Euler potential case we have carried calculations of the Gold-Hoyle branch for the same values L as in the Grad-Shafranov case. The calculations were run for about the same λ range as for the Grad-Shafranov equation, but only one bifurcation point was detected in this range. The λ values of the bifurcation point for all loop lengths is given in Table 2. A comparison with Table 1 shows that the first bifurcation point in the Euler potential case corresponds to the second bifurcation point of the Grad-Shafranov case.

This is also obvious if we plot the λ values of the bifurcation point for different L in the L-λ-plane to compare with the results of De Bruyne and Hood (1992) (see Figure 4). It can clearly be seen that in the Euler potential case it is obviously the first bifurcation which coincides with the stability threshold of linear MHD. This difference between the Grad-Shafranov case and the Euler potential case is surprising and we will discuss the reasons for this in Section 5.

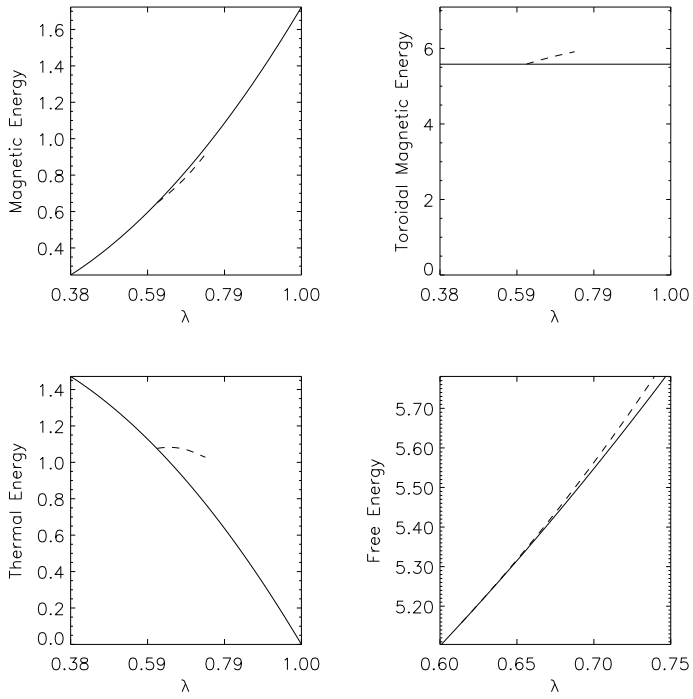

Figure 5. Bifurcation diagrams of the Euler potential case for $L = 7.0$. Shown are the poloidal magnetic energy (upper left), the toroidal magnetic energy (upper right), the thermal energy (lower left) and free energy (lower right). The major differences to Figure 2 are that the bifurcation point shown in this diagram corresponds to the second bifurcation point of the Grad-Shafranov case, and that the bifurcating solution sequence branches off in the direction of increasing λ. This opposite to the Grad-Shafranov case.

Another major difference between the Grad-Shafranov case and the Euler potential case is that in the Euler potential case the new solution sequence branches off towards increasing values of λ, whereas for the Grad-Shafranov case the bifurcating sequence branching off towards decreasing λ values. This has implication for the stability of the bifurcating branch.

For the Euler potential case we define the poloidal magnetic energy as

$$W_{\rm p} = \int \frac{1}{2} \left(\frac{1}{r} \nabla \alpha \right)^2 dV, \tag{34}$$

the toroidal magnetic energy as

$$W_{\rm t} = \int \frac{1}{2} \left(\nabla \alpha \times \nabla \tilde{\beta} \right)^2 dV, \tag{35}$$

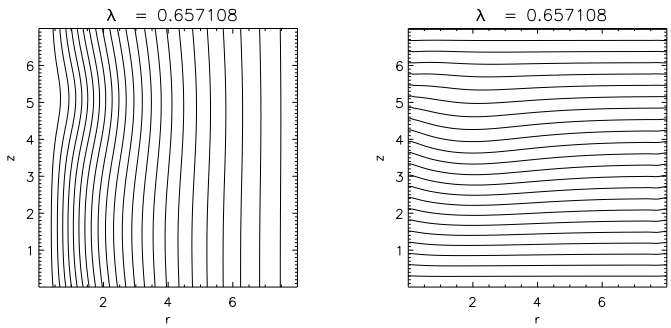

Figure 6. Contour plot of the Euler potentials α (left) and $\tilde{\beta}$ (right) on the bifurcating branch for $\lambda = 0.657$. The spatial structure of α is similar to the spatial structure of A in the Grad-Shafranov case.

the thermal energy as

$$W_{\rm th} = \int p \, dV, \tag{36}$$

and the free energy as

$$W_{\rm f} = W_{\rm p} + W_{\rm t} - W_{\rm th}. \tag{37}$$

One should note that the contribution of the toroidal magnetic energy to the free energy is positive for the Euler potential case, whereas it is negative in the Grad-Shafranov case. The reason for this are the different constraints on the system in the two cases (see Grad, 1964). The poloidal magnetic energy of the bifurcating branch is slightly lower than that of the Gold-Hoyle solution, whereas the toroidal magnetic energy is higher. The thermal energy is also higher than the thermal energy of the Gold-Hoyle solution and the free energy is slightly larger than that of the Gold-Hoyle solution.

The spatial structure of α on the bifurcating branch is similar to the spatial structure of A in the Grad-Shafranov case (see Figure 6; obviously there is no analogue for $\tilde{\beta}$ in the Grad-Shafranov case). In the linear regime α has a $\sin(2\pi z/L)$ z-dependence, whereas $\tilde{\beta}$ has a $1 - \cos(2\pi z/L)$ structure due to Equation (20).

5. Discussion

The results presented in Section 4 raise the following questions.

- Why does the $m = 0$-instability correspond to the second and not to the first bifurcation point in the Grad Shafranove case ?
- Why is the Euler potential case different from the Grad-Shafranov case ?

To answer these questions we first analyse the connection between the line-tying condition in linear ideal MHD stability and the boundary conditions in the Grad-Shafranov and Euler potential cases. Close to the bifurcation points, we can represent the solutions on the bifurcating branches for the Grad-Shafranov case by

$$A_{\rm bif}(r,z,\lambda) = A_{\rm GH}(r,\lambda) + \epsilon A_1(r,z) + \dots \ , \tag{38}$$

where $\epsilon \ll 1$. Note that this expansion differs slightly from the expansion used in the Appendix. To first order in ϵ the function A_1 has to satisfy the equation

$$-\nabla\cdot\frac{1}{r^2}\nabla A_1 = \left(r\frac{d^2p}{dA^2}\Big|_{A_{\rm GH}} + \frac{1}{2r}\frac{d^2b_\phi^2}{dA^2}\Big|_{A_{\rm GH}} \right) A_1, \tag{39}$$

where p and b_ϕ are given by Equations (14) and (15). Since the boundary conditions for $A_{\rm bif}$ are already satisfied by $A_{\rm GH}$, the function A_1 must vanish on all boundaries. Since all coefficients of Equation (39) depend only on r, it is easy to see that the solutions of Equation (39) must be have the form

$$A_1(r,z) = F_n(r)\sin(n\pi z/L), \quad n = 1,2,3,\dots \ , \tag{40}$$

with $F_n(r)$ a radial function.

Close to the bifurcation point, a linear stability analysis of the fundamental Gold-Hoyle branch would give Lagrangian perturbations $\boldsymbol{\xi}$ which are related to A_1 through Equation (25). Since the deviation of the poloidal field from the Gold-Hoyle branch along the bifurcating branch is given by $\nabla\times(A_1\nabla\phi)$, one can easily see that

$$A_1\nabla\phi = -(\boldsymbol{\xi}\cdot\nabla A_{\rm GH})\nabla\phi \tag{41}$$

so that

$$A_1 = -\xi_r\frac{\partial A_{\rm GH}}{\partial r} \tag{42}$$

since $A_{\rm GH}$ depends only on r. Equation (42) shows that the boundary condition $A_1 = 0$ only implies $\xi_r = 0$, but not necessarily $\boldsymbol{\xi} = \mathbf{0}$. We therefore surmise that the first bifurcation in the Grad-Shafranov case corresponds to a linear Lagrangian displacement with non-vanishing ξ_ϕ and/or ξ_z. The solutions on the first branch would satisfy the boundary condition $A_1 = 0$, but not $\boldsymbol{\xi} = \mathbf{0}$. The first bifurcating branch therefore corresponds to solutions which do not satisfy the line-tying boundary conditions, and, for example, can only be reached from the Gold-Hoyle branch if flow through the boundary is allowed ($\xi_z \neq 0$).

The second bifurcating branch satisfies both $A_1 = 0$ and $\boldsymbol{\xi} = \mathbf{0}$. This is corroborated by the fact that the z-dependence of the r-component of the Lagrangian perturbation for the sausage mode is given by $\sin(2\pi z/L)$ (*e.g.* Longbottom *et al.*, 1996). This matches exactly the z-dependence of A_1 on the second bifurcating branch. Therefore the bifurcation points and the linear instability thresholds coincide.

In the Euler potential case, we have boundary conditions for both α and $\tilde{\beta}$, thus constraining the system more than in the Grad-Shafranov case. One can

derive the connection between the Lagrangian perturbation $\boldsymbol{\xi}$ and the linear perturbations α_1 and $\tilde{\beta}_1$ of the Euler potential from the expression for the linear perturbation of the magnetic field,

$$\mathbf{B}_1 = \nabla \times (\boldsymbol{\xi} \times \mathbf{B}_0) = \nabla\alpha_1 \times \nabla\phi + \nabla\alpha_1 \times \nabla\beta_0 + \nabla\alpha_0 \times \nabla\tilde{\beta}_1. \qquad (43)$$

With a bit of algebra one can show (*e.g.* Zwingmann, 1987) that

$$\alpha_1 = -\boldsymbol{\xi} \cdot \nabla\alpha_0, \quad \tilde{\beta}_1 = -\boldsymbol{\xi} \cdot \nabla(\phi + \tilde{\beta}_0), \qquad (44)$$

which for axisymmetric flux tube equilibria like the Gold-Hoyle equilibrium discussed in this paper leads to

$$\alpha_1 = -\xi_r \frac{\partial\alpha_0}{\partial r}, \quad \tilde{\beta}_1 = -\frac{1}{r}\xi_\phi - \xi_z \frac{\partial\tilde{\beta}_0}{\partial z}. \qquad (45)$$

As is to be expected the expression connecting α_1 and ξ_r is the same as for A_1 and ξ_r in the Grad-Shafranov case, and $\alpha_1 = 0$ on the boundaries ensures that $\xi_r = 0$ on the boundaries. The boundary condition $\beta_1 = 0$ imposes an additional constraint, which links ξ_ϕ and ξ_z on the boundaries, ensuring that $\boldsymbol{\xi}_\perp$ vanishes on the boundaries. This is consistent with the line-tying boundary conditions imposed by De Bruyne and Hood (1992) and explains why the bifurcation points coincide with the linear stability threshold in the Euler potential case.

We suspect, but cannot prove, that the different structure of the bifurcation diagrams present in Figures 2 and 5 is also due to the different constraints imposed upon the system by using different descriptions for the magnetic field. The different structure of the bifurcation diagrams may have implication for the stability of the bifurcating equilibrium branch. Usually, when moving along a stable equilibrium sequence and crossing a bifurcation point so that the equilibrium sequence is unstable beyond the bifurcation point, the bifurcating branch is linearly stable close to the bifurcation point if it bifurcates in the forward direction and linearly unstable if it bifurcates in the backward direction (see *e.g.* Iooss and Joseph, 1980). In the present case this would imply that in the Grad-Shafranov case the second bifurcating branch is linearly stable, whereas this branch is unstable in the Euler potential case. This is also supported by the fact that the second bifurcation branch has a lower free energy than the Gold-Hoyle branch for the Grad-Shafranov case, whereas it has a higher free-energy in the Euler potential case. It has to be remarked, however, that this is a conjecture as we have no rigorous proof.

6. Summary and Conclusion

We have investigated the relationship between MHD bifurcation and linear stability for a class of axisymmetric straight flux tubes under line-tying boundary conditions. For simplicity we only considered rotationally symmetric perturbations, allowing only for sausage modes. We have used two different ways of calculating the equilibrium sequences including bifurcating branches - one

approach uses the Grad-Shafranov equation, the other approach uses Euler potentials. It turns out that only the Euler potential case shows a one-to-one correspondence between the first bifurcation point and the linear instability threshold for the sausage mode. The Grad-Shafranov case shows an additional bifurcation which does not correspond to the instability threshold under line-tying boundary conditions. This difference can be explained by the different constraints imposed on the bifurcating equilibrium branches in the Grad-Shafranov and the Euler potential cases.

Furthermore, even though the second bifurcation point of the Grad-Shafranov case coincides with the first bifurcation point of the Euler potential case and the linear instability threshold, the structure of the bifurcation diagrams differ considerably between the Grad-Shafranov and the Euler potential case. The reason for this is not yet clear, but is probably also due to the difference in boundary conditions. In any case this difference has implications for the stability of the bifurcating equilibrium branches (see *e.g.* Iooss and Joseph, 1980) and is therefore important to decide whether the system is able to find a new equilibrium (in the present case a new axisymmetric equilibrium) if one would consider an imaginary process driving the flux tube across the instability threshold.

The present investigation is a preparation for studying equilibrium sequences of magnetic flux tubes and other solar magnetic structures together with their bifurcations in three dimensions. Preliminary steps have already been made (see *e.g.* Romeou and Neukirch, 2002a) and more detailed investigations are planned for the future.

Acknowledgements The authors thank Alan Hood for useful discussions. T. Neukirch acknowledges support by STFC and by the European Commission through the SOLAIRE Network (MTRN-CT-2006-035484). Z. Romeou gratefully acknowledges financial support provided through the European Community's Training and Mobility of Researchers Programme by a Marie-Curie Fellowship and through the European Community's Human Potential Programme under contract HPRN-CT-2000-00153, PLATON. The authors also acknowledge partial support by the British Council ARC Programme.

Appendix

Whereas the first bifurcating branch in the Grad-Shafranov case exists for values of λ which are both bigger and smaller than the λ at the bifurcation point, the second bifurcating branch exists only for λ smaller than the bifurcation λ. This fact can be explained by using standard bifurcation theory to calculate the structure of the bifurcating branches close to the bifurcation points. The argument is actually independent of the form of the functions $p(A)$ and $b_\phi(A)$. The qualitative structure of the bifurcation diagram will thus be the same even if $p(A)$ and $b_\phi(A)$ are changed as long as the fundamental branch consists of solutions which depend only on the radial coordinate r.

We start by writing the Grad-Shafranov equation in the form

$$G(A,\lambda,r) = -r\nabla\cdot\left(\frac{1}{r^2}\nabla A\right) - N(A,\lambda,r) = 0, \tag{46}$$

where the function $N(A, r, \lambda)$ summarizes the nonlinear part of the Grad-Shafranov equation given by $p(A, \lambda)$ and $b_\phi(A, \lambda)$. For the present paper p and b_ϕ are given by Equations (14) and (15). For the following argument, however, the exact form of $N(A, r, \lambda)$ is irrelevant, as long as it is analytic in A and λ at the bifurcation points we want to investigate. We will not give here any details of the mathematical background which can be found for example in Hesse and Schindler (1986) and Hesse and Kiessling (1987) . These papers treat slighly different bifurcation problems, but we will be using the same technique.

Let λ^* be the value of λ at either of the bifurcation points and let $A_0 = A_0(\lambda^*)$ be the solution of Equation (46) at the bifurcation point. To calculate the bifurcating branch we expand λ and A as

$$\lambda = \sum_{k=0}^{\infty} \epsilon^k \lambda_k, \tag{47}$$

$$A = \sum_{k=0}^{\infty} \epsilon^k A_k, \tag{48}$$

where $\lambda_0 = \lambda^*$ and A_0 as above. Since G is analytic in both A and λ for $\lambda > 0$ we can expand Equation (46) in a power series in ϵ:

$$0 = \sum_{k=0}^{\infty} \frac{1}{k!} \frac{d^k}{d\epsilon^k} G(A(\epsilon), \lambda(\epsilon), r)\Big|_{\epsilon=0} \epsilon^k. \tag{49}$$

As each power of ϵ must satisfy this equation independently we obtain

$$\frac{d^k}{d\epsilon^k} G(A(\epsilon), \lambda(\epsilon), r)\Big|_{\epsilon=0} = 0, \qquad k = 0, 1, 2, \dots . \tag{50}$$

Obviously, the lowest order equation

$$G(A_0(\lambda^*), \lambda^*, r) = 0 \tag{51}$$

is just the Grad-Shafranov equation at the bifurcation point and therefore trivially satisfied.

For the discussion of the higher order equations we first have to look at the boundary conditions the A_k have to satisfy. The boundary condtion A_b for $A(r, z, \lambda)$ is given by the fundamental branch solution $A_b(r, z, \lambda) = A_0(r, z, \lambda)$ (the Gold-Hoyle solution in the present paper). Therefore we can extend A_b into the domain. Using the expansion (47) in $A_b(r, z, \lambda(\epsilon))$ we can see that the boundary condition each of the A_k in Equation (48) has to satisfy is given by

$$A_b^{(k)} = \frac{1}{k!} \frac{d^k}{d\epsilon^k} A_0(r, z, \lambda(\epsilon))\Big|_{\epsilon=0}. \tag{52}$$

Note that $A_b^{(k)}$ satifies the same Equation (50) as A_k.

For $O(\epsilon)$ we get from Equation (50)

$$G_A(A_0(\lambda^*), \lambda^*, r) A_1 + G_\lambda(A_0(\lambda^*), \lambda^*, r)\lambda_1 = 0, \tag{53}$$

with

$$G_A A_1 = -r\nabla\cdot\left(\frac{1}{r^2}\nabla A_1\right) - \frac{\partial N}{\partial A}(A_0,\lambda^*,r)A_1, \tag{54}$$

$$G_\lambda = \frac{\partial N}{\partial \lambda}(A_0,\lambda^*,r). \tag{55}$$

As mentioned above $A_b^{(1)}$ satisfies the same equation as A_1 and therefore the function

$$A_1' = A_1 - A_b^{(1)} \tag{56}$$

satisfies $G_A A_1' = 0$ or explicitely

$$-r\nabla\cdot\left(\frac{1}{r^2}\nabla A_1'\right) - \frac{\partial N}{\partial A}(A_0,\lambda^*,r)A_1' = 0 \tag{57}$$

with $A_1' = 0$ on the boundaries. Since all coefficients of Equation (57) depend only on r its solution can be obtained by separation of variables with the general form of A_1' being

$$A_1'(r,z) = F_n(r)\sin(n\pi z/L), \qquad n = 1,2,3,\dots\ . \tag{58}$$

The exact form of $F_n(r)$ is of no importance for the following argument.

If we want to calculate λ_1, we have to go to the next order ($O(\epsilon^2)$) of the expansion, giving

$$-r\nabla\cdot\left(\frac{1}{r^2}\nabla A_2\right) - \frac{\partial N}{\partial A}A_2 - \frac{1}{2}\frac{\partial^2 N}{\partial A^2}A_1^2 - \frac{\partial^2 N}{\partial A\partial\lambda}A_1\lambda_1 - \frac{1}{2}\frac{\partial^2 N}{\partial\lambda^2}\lambda_1^2 - \frac{\partial N}{\partial\lambda}\lambda_2 = 0 \tag{59}$$

where all derivatives of $N(A,\lambda,r)$ are evaluated at the bifurcation point ($\epsilon = 0$). Similarly to $A_b^{(1)}$ at $O(\epsilon)$, $A_b^{(2)}$ satisfies the same equation as A_2. We define

$$A_2' = A_2 - A_b^{(2)} \tag{60}$$

which obeys the equation

$$G_A A_2' = \frac{1}{2}\frac{\partial^2 N}{\partial A^2}({A_1'}^2 + 2A_b^{(1)}A_1') + \lambda_1\frac{\partial^2 N}{\partial A\partial\lambda}A_1'. \tag{61}$$

By Fredholm's alternative the right hand side of Equation (61) has to be orthogonal to A_1', *i.e.*

$$\int_0^L\int_0^{r_{max}}\left(\frac{1}{2}\frac{\partial^2 N}{\partial A^2}({A_1'}^2 + 2A_b^{(1)}A_1') + \lambda_1\frac{\partial^2 N}{\partial A\partial\lambda}A_1'\right)A_1' r dr dz = 0. \tag{62}$$

To proceed we assume in agreement with the Gold-Hoyle solution that the function $A_b^{(1)}$ has the form

$$A_b^{(1)} = \lambda_1 f_b(r) \tag{63}$$

where $f_b(r)$ is left unspecified here. Equation (62) can then be used to calculate λ_1 in the form

$$\lambda_1 \int_0^L \int_0^{r_{max}} \left(\frac{\partial^2 N}{\partial A^2} f_b(r) + \frac{\partial^2 N}{\partial A \partial \lambda} \right) {A_1'}^2 r dr dz = - \int_0^L \int_0^{r_{max}} \frac{1}{2} \frac{\partial^2 N}{\partial A^2} {A_1'}^3 r dr dz. \quad (64)$$

The double integral on the right hand side of Equation (64) can be split into two separate integrations over r and z, since the integrand depends on z only through A_1'. As A_1' has the form (58), the integral over z is given by

$$\int_0^L \sin^3(n\pi z/L) dz = -\frac{L}{n\pi}(\cos n\pi - 1) + \frac{L}{3n\pi}(\cos^3 n\pi - 1), \quad (65)$$

which vanishes for all even n. As the integral on the left hand side of Equation (64) is nonzero, this implies that for even n (and in particular for $n = 2$) λ_1 vanishes. The bifurcation at bifurcation points with modes having even n is therefore quadratic.

This explains the structure of the bifurcation diagram in Figure 2, because the first bifurcation obviously corresponds to the A_1' for $n = 1$, whereas the second bifurcation corresponds to $n = 2$. Therefore the structure of the first branch close to the bifurcation point is given by

$$\lambda = \lambda^* + \epsilon\lambda_1 + \ldots, \quad (66)$$
$$A = A_0(r, z, \lambda^*) + \epsilon A_1(r, z, \lambda^*) + \ldots. \quad (67)$$

The slope of the bifurcating branch at the bifurcation point is determined by $\lambda_1 \neq 0$ in this case and it is obvious that the bifurcating branch exists for both $\lambda > \lambda^*$ ($\epsilon\lambda_1 > 0$) and $\lambda < \lambda^*$ ($\epsilon\lambda_1 < 0$).

Close to the second bifurcation point we have

$$\lambda = \lambda^* + \frac{1}{2}\epsilon^2\lambda_2 + \ldots, \quad (68)$$
$$A = A_0(r, z, \lambda^*) + \epsilon A_1(r, z, \lambda^*) + \ldots, \quad (69)$$

because here λ_1 vanishes. As the correction to λ^* depends quadratically on ϵ, positive and negative ϵ give the same value of λ. This implies that the second bifurcating branch actually consists of *two* branches, one for positive and one for negative ϵ. Since a change of sign of ϵ in Equation (69) corresponds to a simple mirroring of the $\sin(2\pi z/L)$ function at the point $z = L/2$, the two branches have exactly the same energies. We remark that since $\lambda_1 = 0$ in this case $A_1 = A_1'$ as the boundary contribution to A_1' vanishes. The numerical calculations corroborate these results as the same second bifurcation branch is found by the code starting both with negative and positive ϵ. The only difference between the calculations is the mirroring of the z-dependence of A along the bifurcating branch.

References

Allgower, E. L., Georg, K.: 1990, *Numerical Continuation Methods*, Springer, Berlin, p. 7.
Antiochos, S. K., DeVore, C. R., Klimchuk, J. A.: 1999, *Astrophys. J.* **510**, 485.
Arber, T. D., Longbottom, A. W., Van der Linden, R. A. M.: 1999, *Astrophys. J.* **517**, 990.
Barnes, C. W., Sturrock, P. A.: 1972, *Astrophys. J.* **174**, 659.
Bateman, G.: 1978, *MHD Instabilities*, MIT Press, Cambridge MA, p. 68.
Baty, H.: 1997a, *Astron. Astrophys.* **318**, 621.
Baty, H.: 1997b *Solar Phys.* **172**, 249.
Baty, H.: 2000a *Astron. Astrophys.* **353**, 1074.
Baty, H.: 2000b *Astron. Astrophys.* **360**, 345.
Baty, H., Heyvaerts, J.: 1996 *Astron. Astrophys.* **308**, 935.
Becker, U., Neukirch, T., Birk, G. T.: 1996, *Phys. Plasmas* **3**, 1452.
Becker, U., Neukirch, T., Schindler, K.: 2001, *J. Geophys. Res.* **106**, 3811.
Browning, P.K., Gerrard, C., Hood, A.W., Kevis, R., and van der Linden, R.A.M.: 2008, *Astron. Astrophys.* **485**, 837.
Browning, P.K. and Van der Linden, R.A.M.: 2003, *Astron. Astrophys.* **400**, 355.
De Bruyne, P., Hood, A. W.: 1989, *Solar Phys.* **119**, 87.
De Bruyne, P., Hood, A. W.: 1992, *Solar Phys.* **142**, 87.
Edenstrasser, J. W.: 1980a, *J. Plasma Phys.* **24**, 299.
Edenstrasser, J. W.: 1980b, *J. Plasma Phys.* **24**, 515.
Einaudi, G., Van Hoven, G,: 1983, *Solar Phys.* **88**, 163.
Gerrard, C. L., Arber, T. D., Hood, A. W., Van der Linden, R. A. M.: 2001, *Astron. Astrophys.* **373**, 1089.
Grad, H.: 1964, *Phys. Fluids* **7**, 1283.
Gold, T., Hoyle, F.: 1960, *Astrophys. J.* **120** , 89.
Hesse, M.: 1988, *Untersuchungen zur magnetischen Rekonnektion in dreidimensionalen Systemen* , Ph.D. Thesis, Ruhr-Universität Bochum.
Hesse, M., Kiessling, M.: 1987, *Phys. Fluids* **30**, 2720.
Hesse, M., Schindler, K.: 1986, *Phys. Fluids* **29**, 2484.
Hood, A. W., Browning, P.K., Van der Linden, R. A. M.: 2009 *Astron. Astrophys.*, submitted.
Hood, A. W., Priest, E. R.: 1979, *Solar Phys.* **64**, 303.
Hood, A. W., Priest, E. R.: 1981, *Geophys. Astrophys. Fluid Dyn.* **17**, 297.
Hood, A. W., De Bruyne, P., Van der Linden, R. A. M., Goossens, M.: 1994, *Solar Phys.* **150**, 99.
Iooss, G., Joseph, D. D.: 1980, *Elementary Stability and Bifurcation Theory*, Springer, New York, p. 42.
Keller, H. B.: 1977, in P. H. Rabinowitz (ed.), *Applications of Bifurcation Theory*, Academic Press, New York, p. 359.
Kiessling, M.K.-H. and Neukirch, T.: 2003, *Proc. Natl. Acad. Sci.* **100**, 1510.
Lionello, R., Velli, M., Einaudi, G., Mikić, Z.: 1998, *Astrophys. J.* **494**, 840.
Longbottom, A.W., Hood, A.W., Rickard, G.: 1996, *Plasma Phys. Control. Fusion* **38**, 193.
Mikić, Z., Schnack, D. D., Van Hoven, G.: 1990, *Astrophys. J.* **361**, 690.
Neukirch, T.: 1993a, *J. Geophys. Res.* **98**, 3753.
Neukirch, T.: 1993b, *Astron. Astrophys.* **274**, 319.
Neukirch, T. and Hesse, M.: 1993, *Astrophys. J.* **411**, 840.
Priest, E. R.: 1982, *Solar Magnetohydrodynamics*, D. Reidel, Dordrecht.
Platt, U., Neukirch, T.: 1994, *Solar Phys.* **153**, 287.
Raadu, M. A.: 1972, *Solar Phys.* **22**, 425.
Romeou, Z. and Neukirch, T.: 1999, In: Wilson, A. (ed.), *Magnetic Fields and Solar Processes, ESA-SP 448*, 871.
Romeou, Z. and Neukirch, T.: 2001, In: Hanslmeier, A., Messerotti, M., Veronig, A. (eds.), *The Dynamic Sun*, Kluwer Academic Publishers, Dordrecht, 303.
Romeou, Z. and Neukirch, T.: 2002a, *J. Atmos. Solar Terr. Phys.* **64**, 639.
Romeou, Z. and Neukirch, T.: 2002b, In: Sawaya-Lacoste, H. (ed.), *Proc. SOLMAG: Magnetic Coupling of the Solar Atmosphere Euroconference, ESA-SP 505*, 549.
Rosner, R., Low, B. C., Tsinganos, K., Berger, M. A.: 1989, *Geophys. Astrophys. Fluid Dyn.* **48**, 251.
Schindler, K., Birn, J., Janicke, L.: *Solar Phys.* **87**, 103.
Schröer, A., Neukirch, T., Kiessling, M. K.-H., Hesse, M., Schindler, K.: 1994, *Phys. Plasmas* **1**, 213.

Solovev, L. S.: 1967, in M. A. Leontovich (ed.), *Reviews of Plasma Physics* **3**, Consultans Bureau, New York, p. 277.
van der Linden, R.A.M. and Hood, A.W.: 1998, *Astron. Astrophys.* **339**, 887.
van der Linden, R.A.M. and Hood, A.W.: 1999, *Astron. Astrophys.* **346**, 303.
Velli, M., Hood, A. W., Einaudi, G.: 1990, *Astrophys. J.* **350**, 428.
Zwingmann, W.: 1983, *J. Geophys. Res.* **88**, 9101.
Zwingmann, W.: 1987, *Solar Phys.* **111**, 309.